Equilibrium running principle analysis on an adaptive cycle engine

Zheng, Junchao; Tang, Hailong; Chen, Min; Yin, Feijia

DOI
10.1016/j.applthermaleng.2017.12.102

Publication date
2017

Document Version
Final published version

Published in
Applied Thermal Engineering

Applied Thermal Engineering 132 (2018) 393–409

Contents lists available at ScienceDirect

Applied Thermal Engineering

journal homepage: www.elsevier.com/locate/apthermeng

Research Paper

Equilibrium running principle analysis on an adaptive cycle engine

Junchao Zheng [a], Hailong Tang [a], Min Chen [a,*], Fei-Jia Yin [b]

[a] School of Energy and Power Engineering, Beihang University, Beijing 100191, China
[b] Aircraft Noise and Climate Effects, Delft University of Technology, Leeghwaterstraat 44, 2628 CA Delft, The Netherlands

HIGHLIGHTS

- The adaptive cycle engine is an evolutional concept of variable cycle engine.
- The advantages of the adaptive cycle engine depend on the matching principles.
- The equilibrium running principles of the adaptive cycle engine are deduced.
- A nonlinear component-based adaptive cycle engine performance model is built.
- The application of the equilibrium running principles based on model is proposed.

ARTICLE INFO

Article history:
Received 13 September 2017
Revised 5 December 2017
Accepted 26 December 2017
Available online 27 December 2017

Keywords:
Adaptive cycle engine
Components matching principle
Variable cycle engine
Overall performance

ABSTRACT

As an evolutional concept of variable cycle engine, the adaptive cycle engine draws widely attention with high expectations. It combines a variable geometry schedule and component matching principles to demonstrate its advantages such as avoiding severe inlet spillage drag and the wide variable cycle characteristics. Thus, this paper aims at equilibrium running principle analysis on an adaptive cycle engine at variable operating modes, deriving the equilibrium running equations of an adaptive cycle engine for the first time, and exploring the physical essence of components matching principle on the basis of a newly developed nonlinear component-based adaptive cycle engine performance model. It uncovers the physical essence of components matching relationships and provides mathematical derivation of equilibrium running principles which lay theoretical foundation of the variable geometries modulation schedule and overall performance optimization on an adaptive cycle engine.

1. Introduction

For the next generation of affordable aircraft, all-weather, long-range, multi-mission tend to be new design objectives [1–3]. These design objectives lead to new requirements on aircraft engine design. The inherent contradictions of typical turbojets and turbofans are difficult to be solved: the newly designed engine should have the turbojet feature such as higher specific thrust in order to be qualified for the thrust stringent mission such as non-augmented supersonic cruising and transonic climbing; it also should have the turbofan feature of lower specific fuel consumption to compete in the fuel cost mission [4] such as long-range reconnaissance [5]. To achieve these conflicting goals in a gas turbine [6], the VCEs (variable cycle engines) [7–10] tend to be the advanced and popular propulsion devices.

As an evolutional concept of VCE, the ACE [11–13] (adaptive cycle engine) draws widely attention with high expectations. It consists of a typical double bypass VCE surrounded by an additional bypass duct. So, it has a CDFS (core driven fan stage) on the HP (high pressure) rotor in front of a HPC (high pressure compressor) and two VABIs (variable area bypass injectors, Pro-VABI means the front one, Rear-VABI means the rear one). This derived bypass duct contains a row of VSVs (variable stator vanes) and a single compression stage through extending one row of main fan blades into the stream. This new configuration is called ‘Flade’, which is created from ‘Fan on blade’. In essence, the ACE is a triple bypass variable cycle engine. The configuration of an ACE is shown in Fig. 1. In order to distinguish such complex bypass ducts, the bypass behind the CDFS is defined as ‘First Bypass’, the one behind the fan is ‘Second Bypass’, while the new one is ‘Third Bypass’. Through different combined adjustment schedules of several variable geometries, an ACE can be divided artificially into four different operating modes while a typical double bypass VCE has only two modes. When all the bypasses are open, it operates at triple

* Corresponding author at: BeiHang University, XueYuan Road No.37, HaiDian District, Beijing 100191, China.
E-mail address: chenmin@buaa.edu.cn (M. Chen).

https://doi.org/10.1016/j.applthermaleng.2017.12.102
1359-4311/

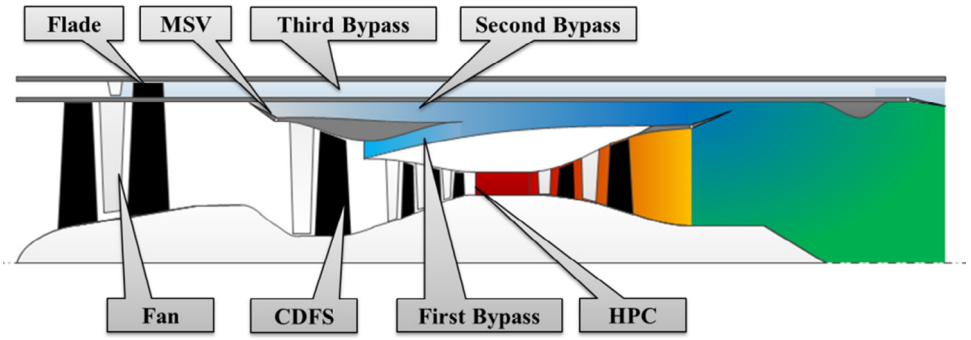

Fig. 1. The configuration of an ACE with Flade.

bypass mode named Mode M3. When the third bypass is closed while the second bypass is open, it operates at double bypass mode named Mode M2. On the contrary, if the third bypass is open while the second bypass is closed, it operates at other different double bypass mode named Mode M13. When only the first bypass is open, it is called one bypass mode named Mode M1. Specially, when an ACE operates at Mode 1 or Mode 2, the third bypass just opens a little which guarantees the flow continuity but affects little to the power balance.

Initially, compared with typical aero-engines, avoiding severe inlet spillage drag at supersonic part-load operation and greater variable cycle characteristics are the two obvious advantages of an ACE. Furthermore, by allowing the engine to pass as much amount of air as possible at part-load operation during supersonic cruise, an ACE can avoid severe inlet spillage drag versus the typical double bypass VCE. In addition, the alternatives of four different operating modes can extend the range of engine bypass ratio variation enormously. These advantages can only be demonstrated through proper combined variable geometries control schedule design and rational components matching principle of an ACE. Some researchers have made some progress on this. The literature [12] aims to predict and discuss the effect of each variable geometries modulation on the matching relationship between engine components as well as the overall engine performance at different operating modes. The aim of literature [13] is to study the variable geometries modulation schedule of an ACE (The configuration of the ACE is shown in Fig. 2) in maintaining airflow during throttling. Relative results show that the overall airflow of an ACE remains constant with improved SFC (specific fuel consumption) even though net thrust decreases by about 32% during supersonic cruise, while the airflow of conventional ATF (advanced turbofan) reduces by 18%. Meanwhile, when the engine thrust reduces from 100% to 50% during subsonic cruise, the ACE engine maintains a constant engine airflow with improved SFC, while the airflow of conventional ATF reduces by 30%. The above two literatures aim at investigating the effect of each variable geometries modulation on the matching relationship between engine components as well as the overall engine performance at different operating modes.

However, in the existing literatures, there is no public literature to uncover the physical essence of components matching relationships and provide mathematical derivation of equilibrium running principle of an ACE. It urgently needs to study them mentioned above, which can lay theoretical foundation on the variable geometries modulation schedule and performance analysis on an ACE. Therefore, this paper aims at equilibrium running principle analysis on an ACE at variable operating modes, deriving the equilibrium running equations of an ACE and exploring the physical essence of components matching principle for the first time.

The ACE performance model is a zero-dimensional model which can be used for parametric cycle analysis, performance analysis [14], control schedule [15] study and so on. The engine performance model is established by a set of interconnected gas components. The performance of these components is expressed in terms of characteristic maps or empirical formulas. Every component is considered as a 'black box' whose inlet section and outlet section is defined for modeling. For passing information between related components, a series of gas thermodynamic parameters such as mass flow, pressure (total or static), temperature (total or static), velocity coefficient (or Mach number), fuel-air ratio, enthalpy, etc. are defined at each section. These mentioned parameters can be solved numerically by thermodynamic calculation via related formulas. More details of general zero-dimensional aero- engine performance modeling can be found in these references [16–20].

To improve the performance model precision, gas property differences are considered in the model via variable specific heat capacity calculation. These differences are caused by the variation of gas ingredient, temperature, humidity and so on. Other measures are also adopted effectively for example of altitude, Mach number, power extraction, cooling air circulation.

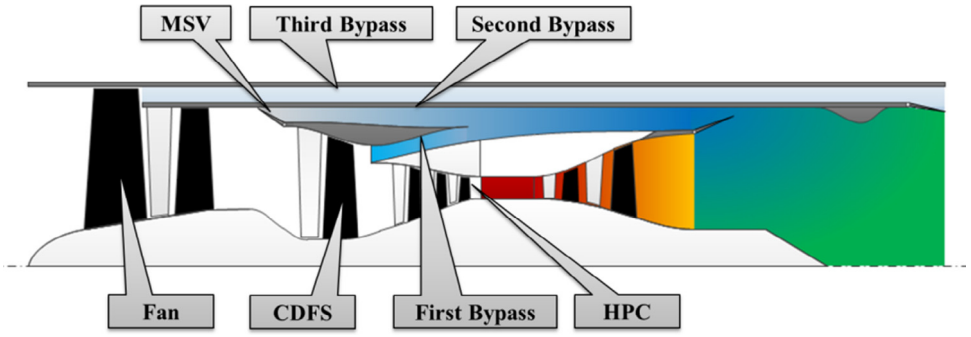

Fig. 2. The configuration of an ACE with front fan.

In this article, 'Introduction' section gives a brief introduction on the background of an ACE. Section 'Equilibrium running Principle Analysis on an ACE at Variable Operating modes' discusses the equilibrium running principle at various modes of an ACE via the HP or LP (low pressure) rotor equilibrium running equations derivation on an ACE at variable operating modes. Then, the ace performance modeling is introduced. The next section is about the equilibrium running application analysis on an ACE via the ACE performance model. Final section draws the conclusions.

2. Equilibrium running principle analysis on an ACE at variable operating modes

In order to analyze the equilibrium running principle of an ACE, the related sections are defined as Fig. 3. Details are shown in Table 1.

The first bypass split ratio is defined as below:

$$B_1 = \frac{W_{a24}}{W_{a23}} \tag{1}$$

where B_1 is the first bypass split ratio, W_{a24} is the first bypass air flow (kg/s), and W_{a23} is the HPC air flow (kg/s).

The second bypass split ratio is defined as below:

$$B_2 = \frac{W_{a22}}{W_{a21}} \tag{2}$$

where B_2 is the second bypass split ratio, W_{a22} is the second bypass air flow (kg/s), and W_{a21} is the CDFS air flow (kg/s).

The third split bypass split ratio is defined as below:

$$B_3 = \frac{W_{a12}}{W_{a2}} \tag{3}$$

where B_3 is the third bypass split ratio, W_{a12} is the third bypass air flow (kg/s), and W_{a2} is the fan air flow (kg/s).

According to these definitions, the total bypass ratio can be expressed as below:

$$B = \frac{W_{a24} + W_{a22} + W_{a12}}{W_{a23}} = B_1 + B_2(1 + B_1) + B_3(1 + B_2)(1 + B_1) \tag{4}$$

where B is the total bypass ratio.

2.1. Equilibrium running principle theoretical basis on an ACE

When a gas turbine engine works at off-design conditions, the HP or LP rotor components should satisfy the mutual interaction relationships. That is called equilibrium running conditions which are listed as below:

(1) Flow continuity. Specifically, as an ACE has multiple gas flow splitting and mixing situations, the HP or LP rotor flow continuity is more complex compared with a turbofan.

Table 1
Definitions for related sections of ACE.

Number	Section
12	The Flade inlet
13	The Flade outlet
18	The third bypass nozzle
2	The fan inlet
21	The CDFS inlet
22	The second bypass outlet
23	The HPC inlet
24	The first bypass inlet
25	The Pro-VABI outlet
3	The HPC outlet
4	The HPT inlet
5	The LPT inlet
52	The mixer bypass inlet
55	The LPT outlet
6	The mixer outlet
7	The afterburner outlet
8	The nozzle throat section

(2) Power balance in a rotor. An ACE adds new compression components such as the Flade compared with a VCE or a turbofan.
(3) Rotational speed equality on corresponding rotors.
(4) Pressure balance at flow mixed sections.

Although an ACE is much more complex than other typical gas turbine aero-engines, it should also observe these basic equilibrium running conditions mentioned above. So, the HP and LP rotor equilibrium running equations of an ACE at variable operating modes can be deduced. They are the mathematical expressions of the equilibrium running relationships.

2.2. HP rotor equilibrium running equation derivation of an ACE

When an ACE works at these four operating modes, its HP rotor components are the CDFS, the HPC and the HPT (high pressure turbine). The first bypass keeps open. The flow from the CDFS outlet splits into the HPC inlet and the first bypass duct. So, the HP rotor equilibrium running equations of an ACE at all the four operating modes are the same. The HP rotor flow continuity and power balance relationships of an ACE are deduced as below.

According to Eq. (1) and ignoring the fuel flow, the flow continuity equation between the CDFS inlet and the HPT inlet can be defined as below:

$$W_{a21}\frac{1}{1 + B_1} \approx W_{g4} \tag{5}$$

where W_{g4} is the HPT inlet gas flow (kg/s).

The mentioned two flows can also be expressed by the flow function on aerodynamics:

$$W_{a21} = KA_{21}\frac{p_{t21}}{\sqrt{T_{t21}}}q(\lambda_{21}) \tag{6}$$

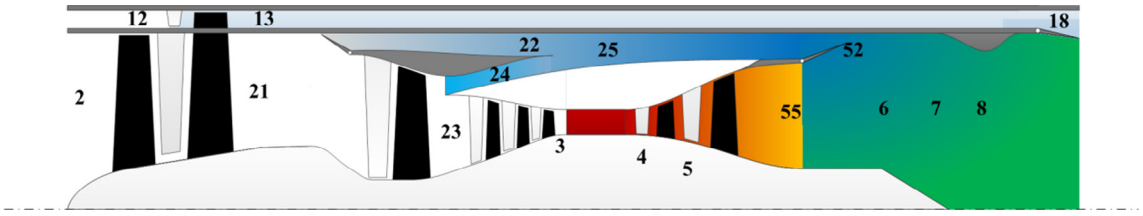

Fig. 3. Introduction of related sections of ACE (these section definitions are shown in Table 1).

where K is the air flow function constant, A_{21} is the CDFS inlet area (m^2), p_{t21} is the CDFS inlet total pressure (Pa), T_{t21} is the CDFS inlet total temperature (K), $q(\lambda_{21})$ is the CDFS inlet flow function which is the function of the velocity coefficient of the CDFS inlet section (λ_{21}).

$$W_{g4} = K_g A_4 \frac{p_{t4}}{\sqrt{T_{t4}}} q(\lambda_4) \tag{7}$$

where K_g is the gas flow function constant, A_4 is the HPT inlet area (m^2), p_{t4} is the HPT inlet total pressure (Pa), T_{t4} is the HPT inlet total temperature (K), $q(\lambda_4)$ is the HPT inlet flow function which is the function of the velocity coefficient of the HPT inlet section (λ_4).

On the basis of the expressions of the CDFS and the HPC pressure ratios, the total pressure ratio between the CDFS inlet section and the HPT inlet section can be expressed as below:

$$\frac{p_{t4}}{p_{t21}} = \pi_{CDFS}\pi_{HPC}\sigma_{21\to4} \tag{8}$$

where π_{CDFS} is the CDFS pressure ratio, π_{HPC} is the HPC pressure ratio, $\sigma_{21\to4}$ is the CDFS inlet to HPT inlet total pressure recovery coefficient.

Integrating and transforming Eqs. (5)–(7), the HP rotor flow continuity equation is established. Eq. (9) is based on the CDFS inlet section, while Eq. (10) is based on the HPC inlet section. Eq. (11) describes the relationship between the first bypass split ratio and the CDFS pressure ratio.

$$\pi_{CDFS}\pi_{HPC} = \frac{KA_{21}}{K_g A_4 q(\lambda_4)\sigma_{21\to4}} \cdot \frac{1}{1+B_1}\sqrt{\frac{T_{t4}}{T_{t21}}} q(\lambda_{21}) \tag{9}$$

$$\pi_{HPC} = \frac{KA_{23}}{K_g A_4 q(\lambda_4)\sigma_{21\to4}} \cdot \sqrt{\frac{T_{t4}}{T_{t23}}} q(\lambda_{23}) \tag{10}$$

where A_{23} is the HPC inlet area (m^2), T_{t23} is the HPC inlet total pressure (Pa), $q(\lambda_{23})$ is the HPC inlet flow function which is the function of the velocity coefficient of the HPC inlet section (λ_{23}).

$$B_1 + 1 = \frac{A_{21}}{A_{23}} \cdot \frac{q(\lambda_{21})}{q(\lambda_{23})} \cdot \pi_{CDFS} \cdot \sqrt{\frac{T_{t23}}{T_{t21}}} \tag{11}$$

The HP rotor power balance is expressed by Eq. (12) as below:

$$(L_{HPC} + L_{CDFS})W_{a23} + L_{CDFS}W_{a24} = \eta_{mH}W_{g4}L_{HPT} \tag{12}$$

where L_{HPC} is the HPC unit power (J/kg), L_{CDFS} is the CDFS unit power (J/kg), η_{mH} is the HP Rotor mechanical efficiency, L_{HPT} is the HPT unit power (J/kg).

Considering flow split relationship between the CDFS and the HPC, Eq. (12) varies to Eq. (13) when the HP rotor mechanical efficiency and fuel flow are ignored.

$$L_{CDFS}(1 + B_1) + L_{HPC} \approx L_{HPT} \tag{13}$$

According to the compression work equation, the unit power of the CDFS, the HPC and the HPT can be described as Eqs. (14)–(16).

$$L_{CDFS} = \frac{1}{\eta_{CDFS}} c_p T_{t21}(e_{CDFS} - 1) \tag{14}$$

where η_{CDFS} is the CDFS efficiency, c_p is the specific heat at constant pressure (J/(kg·K)), e_{CDFS} is the function of the CDFS pressure ratio shown in Eq. (17).

$$L_{HPC} = \frac{1}{\eta_{HPC}} c_p T_{t23}(e_{HPC} - 1) \tag{15}$$

where η_{HPT} is the HPT efficiency, e_{HPC} is the function of the HPC pressure ratio shown in Eq. (17).

$$L_{HPT} = \eta_{HPT} c_p T_{t4}\left(1 - \frac{1}{e_{HPT}}\right) \tag{16}$$

where η_{HPC} is the HPC efficiency, e_{HPT} is the function of the HPT pressure ratio shown in Eq. (17).

$$e = \pi^{\frac{k-1}{k}} \tag{17}$$

where e is the pressure ratio function, π is the pressure ratio, k is the adiabatic exponent.

As the unit power of the CDFS and the HPC are based on different sections, it is difficult to establish the power balance equation. It needs Eq. (18) to establish the relation between the total temperature of the CDFS and the HPC inlet sections.

$$T_{t23} = T_{t21}\left[1 + \frac{1}{\eta_{CDFS}}(e_{CDFS} - 1)\right] \tag{18}$$

Uniting Eqs. (13)–(16), the HP power balance equation is established: Eq. (19) refers to the HPC inlet section while Eq. (20) refers to the CDFS section.

$$\frac{T_{t4}}{T_{t21}} = \frac{1}{\eta_{HPT}\left(1 - \frac{1}{e_{HPT}}\right)}\left[\frac{e_{HPC} - 1}{\eta_{HPC}}\left(1 + \frac{e_{CDFS} - 1}{\eta_{CDFS}}\right) + (1 + B_1)\frac{e_{CDFS} - 1}{\eta_{CDFS}}\right] \tag{19}$$

$$\frac{T_{t4}}{T_{t23}} = \frac{1}{\eta_{HPT}\left(1 - \frac{1}{e_{HPT}}\right)}\left[\frac{e_{HPC} - 1}{\eta_{HPC}} + (1 + B_1)\frac{1}{1 + \frac{\eta_{CDFS}}{e_{CDFS} - 1}}\right] \tag{20}$$

Combined with Eqs. (9) and (19), the HP rotor equilibrium running equation is established as Eq. (21). Similarly, Eq. (23) is established by Eqs. (10) and (20). Eq. (21) is based on the CDFS inlet section which can be used to the CDFS equilibrium running analysis, while Eq. (23) refers to HPC. When the HPT (high pressure turbine) variable area nozzle is fixed, the defined variable value in Eq. (22) is constant. It should be pointed out that, when t the factors in the square root belongs to second order effects in Eqs. (21) and (23). According to Eq. (21), in order to satisfying the HP equilibrium running equation, it is a negative correlation between the first bypass split ratio and the pressure ratios of HPC and CDFS.

$$\frac{1}{B_1 + 1}\frac{q(\lambda_{21})A_{21}}{\pi_{CDFS}\pi_{HPC}}\sqrt{\frac{1}{\eta_{HPT}\left(1 - \frac{1}{e_{HPT}}\right)}} \times \sqrt{\frac{e_{HPC} - 1}{\eta_{HPC}}\left(1 + \frac{e_{CDFS} - 1}{\eta_{CDFS}}\right) + (1 + B_1)\frac{e_{CDFS} - 1}{\eta_{CDFS}}} = C_H \tag{21}$$

$$C_H = \frac{K_g A_4 q(\lambda_4)\sigma_{21\to4}}{K} \tag{22}$$

$$\frac{q(\lambda_{23})A_{23}}{\pi_{HPC}}\sqrt{\frac{1}{\eta_{HPT}\left(1 - \frac{1}{e_{HPT}}\right)}}\sqrt{\frac{e_{HPC} - 1}{\eta_{HPC}} + (1 + B_1)\frac{1}{1 + \frac{\eta_{CDFS}}{e_{CDFS} - 1}}} = C_H \tag{23}$$

Comparing Eqs. (21) and (23), the first bypass split ratio can be expressed by Eq. (24). It reflects the influences from the pressure ratios of the HPC and the CDFS to the first bypass split ratio.

$$B_1 + 1 = \frac{A_{21}}{A_{23}} \cdot \frac{q(\lambda_{21})}{q(\lambda_{23})} \cdot \frac{1}{\pi_{CDFS}} \cdot \sqrt{1 + \frac{e_{CDFS} - 1}{\eta_{CDFS}}} \tag{24}$$

2.3. LP (low pressure) rotor equilibrium running equation derivation at Mode M1 of an ACE

The LP flow continuity equation derivation at Mode M1 of an ACE is similar to the HP flow continuity equation derivation. The LP flow continuity equation is Eq. (25).

$$\pi_{Fan}\pi_{CDFS}\pi_{HPC} = \frac{KA_2\pi_{HPT}}{K_g A_5 q(\lambda_5)\sigma_{2-5}} \cdot \sqrt{\frac{T_{t5}}{T_{t2}}} q(\lambda_2) \frac{1}{B_1+1} \tag{25}$$

where π_{Fan} is the fan pressure ratio, A_2 is the fan inlet area (m^2), π_{HPT} is the HPT expansion ratio, A_5 is the LPT inlet area (m^2), $q(\lambda_5)$ is the LPT inlet flow function which is the function of the velocity coefficient of the HPC inlet section (λ_5), σ_{2-5} is the fan inlet to LPT inlet total pressure recovery coefficient, T_{t5} is the LPT inlet total temperature (K), T_{t2} is the fan inlet total temperature (K), $q(\lambda_2)$ is the fan inlet flow function which is the function of the velocity coefficient of the HPC inlet section (λ_2).

The LP power balance equation derivation at Mode M1 of an ACE is also similar to the HP power balance equation. Eq. (26) is LP power balance equation at Mode M1 of an ACE. Compared with Eqs. (19) and (20), the first bypass split ratio has an impact on both the HP and LP flow continuity.

$$\frac{T_{t5}}{T_{t2}} = \frac{1+B_1}{\eta_{\mathrm{LPT}}\eta_{\mathrm{Fan}}}(e_{\mathrm{Fan}}-1)\frac{1}{1-1/e_{LPT}} \tag{26}$$

where η_{LPT} is the LPT efficiency, η_{Fan} is the fan efficiency, e_{Fan} is the function of the fan pressure ratio shown in Eq. (17), e_{LPT} is the function of the LPT pressure ratio shown in Eq. (17).

Combined with Eqs. (25) and (26), the LP equilibrium running equation at Mode M1 (Eq. (27)) is established. When the LPT (low pressure turbine) variable area nozzle is fixed, the defined variable value in Eq. (28) is constant The HPT pressure ratio remains unchanged.

$$\pi_{\mathrm{Fan}}\pi_{CDFS}\pi_{\mathrm{HPC}} = C_L \cdot \sqrt{\frac{1}{\eta_{\mathrm{Fan}}(1+B_1)}(e_{\mathrm{Fan}}-1)} \cdot \sqrt{\frac{1}{(1-1/e_{LPT})\eta_{LPT}}} \cdot q(\lambda_2)A_2 \tag{27}$$

$$C_L = \frac{K\pi_{HPT}}{K_g A_5 q(\lambda_5)\sigma_{2-5}} \tag{28}$$

2.4. LP rotor equilibrium running equation derivation at Mode M13 of an ACE

When an ACE operates at Mode M13, the third bypass is open. The air from engine inlet splits into two section: the fan inlet section (Section 2, shown in Table 1) and the Flade inlet section (Section 12). So, the LP flow continuity equation at Mode M13 can be established based on two different mentioned sections. This is similar to the HP equilibrium running equation of an ACE. The LP flow continuity equation at Mode M13 based on the fan inlet section is the same with Mode M1 shown in Eq. (25). While, the LP flow continuity equation at Mode M13 based on the Flade inlet section is shown in Eq. (29). The difference between the two LP flow continuity equations at Mode M13 is t the third bypass split ratio.

$$\pi_{Fan}\pi_{CDFS}\pi_{HPC} = \frac{KA_{12}\pi_{HPT}}{K_g A_5 q(\lambda_5)\sigma_{2-5}} \cdot \sqrt{\frac{T_{t5}}{T_{t12}}} q(\lambda_{12}) \frac{1}{B_1+1} \cdot \frac{1}{B_3} \tag{29}$$

where A_{12} is the Flade inlet area (m^2), T_{t12} is the Flade inlet total temperature (K), $q(\lambda_{12})$ is the Flade inlet flow function which is the function of the velocity coefficient of the HPC inlet section (λ_{12}).

As the fan inlet total temperature is identical with the Flade inlet total temperature, the LP power balance equation at Mode M13 of an ACE evolves into Eq. (30).

$$\frac{T_{t5}}{T_{t2}} = \frac{1+B_1}{\eta_{LPT}}\left(\frac{e_{Fan}-1}{\eta_{Fan}} + \frac{e_{Flade}-1}{\eta_{Flade}}B_3\right)\frac{1}{1-1/e_{LPT}} \tag{30}$$

where e_{Flade} is the function of the Flade pressure ratio shown in Eq. (17), η_{Flade} is the Flade efficiency.

The LP equilibrium running equation at Mode M13 is established by the LP flow continuity equation at Mode M13 (Eq. (25) or Eq. (29)) and the LP power balance equation at Mode M13 (Eq. (30)). In detail, Eq. (31) is based on the fan inlet section while Eq. (32) is based on the Flade inlet section. Compared with the LP equilibrium running equation at Mode M1 (Eq. (27)), the LP equilibrium running equations at Mode M13 (Eqs. (31) and (32)) are more complex for the influences of the Flade and the third bypass split ratio. According to Eq. (32), it is a negative correlation between the third bypass split ratio and the Fan, HPC or CDFS pressure ratios.

$$\pi_{Fan}\pi_{CDFS}\pi_{HPC} = C_L \cdot \sqrt{\frac{1}{B_1+1}\left(\frac{e_{\mathrm{Fan}}-1}{\eta_{\mathrm{Fan}}} + \frac{e_{Flade}-1}{\eta_{Flade}}B_3\right)} \cdot \sqrt{\frac{1}{(1-1/e_{LPT})\eta_{LPT}}} \cdot q(\lambda_2)A_2 \tag{31}$$

$$\pi_{Fan}\pi_{CDFS}\pi_{HPC} = C_L \cdot \sqrt{\frac{1}{B_1+1}\left(\frac{e_{\mathrm{Fan}}-1}{\eta_{\mathrm{Fan}}} + \frac{e_{Flade}-1}{\eta_{Flade}}B_3\right)} \cdot \sqrt{\frac{1}{(1-1/e_{LPT})\eta_{LPT}}} \cdot \frac{q(\lambda_{12})A_{12}}{B_3} \tag{32}$$

2.5. LP rotor equilibrium running equation derivation at Mode M2 of an ACE

When an ACE operates at Mode M2, the second bypass is open. So, the Fan outlet air can flow into CDFS or the second bypass. Considering this effects, the LP flow continuity equation (Eq. (33)) and the power balance equation (Eq. (34)) at Mode M2 is quite different with the related equations at Mode M1. The two mentioned equations are influenced by the second bypass split ratio.

$$\pi_{Fan}\pi_{CDFS}\pi_{HPC} = \frac{KA_2\pi_{\mathrm{HPT}}}{K_g A_5 q(\lambda_5)\sigma_{2-5}} \cdot \sqrt{\frac{T_{t5}}{T_{t2}}} q(\lambda_2) \frac{1}{B_1+1}\frac{1}{B_2+1} \tag{33}$$

$$\frac{T_{t5}}{T_{t2}} = \frac{(1+B_1)(1+B_2)}{\eta_{\mathrm{LPT}}\eta_{\mathrm{Fan}}}(e_{\mathrm{Fan}}-1)\frac{1}{1-1/e_{LPT}} \tag{34}$$

Similarly, the LP equilibrium running equation at Mode M2 (Eq. (35)) is established by the LP flow continuity equation (Eq. (33)) and the power balance equation (Eq. (34)) at Mode M2. The LP equilibrium running equation at Mode M2 reflects additional effects which is the second bypass split ratio versus the equation at Mode M1 (Eq. (27)). According to Eq. (35), it is a negative correlation between the second bypass split ratio and the pressure ratios of the Fan, the HPC or the CDFS.

$$\pi_{\mathrm{Fan}}\pi_{CDFS}\pi_{\mathrm{HPC}} = C_L \cdot \sqrt{\frac{1}{\eta_{\mathrm{Fan}}(B_1+1)(B_2+1)}(e_{\mathrm{Fan}}-1)} \cdot \sqrt{\frac{1}{(1-1/e_{LPT})\eta_{LPT}}} \cdot q(\lambda_2)A_2 \tag{35}$$

2.6. LP rotor equilibrium running equation derivation at Mode M3 of an ACE

When an ACE operates at Mode M3, all the bypasses are open. So, this operating mode has all the characteristics of the other operating modes. The LP flow continuity equations at Mode M3 also have two different expressions compared with the equations at Mode M13. Specifically, one is based on the fan inlet section which is the same with the LP flow continuity equation at Mode M2 (Eq. (33)). The other is based on the Flade inlet section shown in Eq. (36).

$$\pi_{Fan}\pi_{CDFS}\pi_{HPC} = \frac{KA_{12}\pi_{\mathrm{HPT}}}{K_g A_5 q(\lambda_5)\sigma_{2-5}} \cdot \sqrt{\frac{T_{t5}}{T_{t12}}} q(\lambda_{12}) \frac{1}{B_1+1} \cdot \frac{1}{B_2+1} \frac{1}{B_3} \tag{36}$$

As all LP compression components (the fan and the Flade) operate at Mode M3, the LP power balance equation at Mode M3 (Eq. (37)) has more factors compared with the equation at Mode M13 or M2. It adds the effect of the second bypass split ratio versus the equation at Mode M13. Meanwhile it considers the Flade power versus the equation at Mode M2.

$$\frac{T_{t5}}{T_{t2}} = \frac{(1+B_1)(1+B_2)}{\eta_{LPT}} \left(\frac{e_{Fan}-1}{\eta_{Fan}} + \frac{e_{Flade}-1}{\eta_{Flade}} B_3 \right) \frac{1}{1-1/e_{LPT}} \tag{37}$$

United the LP flow continuity equations at Mode M3 (Eq. (33) or Eq. (36)) and the power balance equation (Eq. (37)), the LP equilibrium running equations at Mode M3 are established shown as below: Eq. (38) is based on the Fan inlet section and Eq. (39) is based on the Flade inlet section.

$$\pi_{\mathrm{Fan}}\pi_{CDFS}\pi_{\mathrm{HPC}} = C_L \cdot \sqrt{\frac{1}{(1+B_1)(1+B_2)} \left(\frac{e_{Fan}-1}{\eta_{Fan}} + \frac{e_{Flade}-1}{\eta_{Flade}} B_3 \right)} \cdot \sqrt{\frac{1}{(1-1/e_{LPT})\eta_{LPT}}} \cdot q(\lambda_2) A_2 \tag{38}$$

$$\pi_{\mathrm{Fan}}\pi_{CDFS}\pi_{\mathrm{HPC}} = C_L \cdot \sqrt{\frac{1}{(1+B_1)(1+B_2)} \left(\frac{e_{Fan}-1}{\eta_{Fan}} + \frac{e_{Flade}-1}{\eta_{Flade}} B_3 \right)} \cdot \sqrt{\frac{1}{(1-1/e_{LPT})\eta_{LPT}}} \cdot \frac{q(\lambda_{12}) A_{12}}{B_3} \tag{39}$$

2.7. Equilibrium running equations analysis at various modes of an ACE

Compared with the conventional double shaft mixed turbofan HP rotor equilibrium running equation (Eq. (40)), the HP rotor equilibrium running equation of an ACE (Eq. (23)) gains additional factors: the CDFS and the first bypass split ratio. The first bypass split ratio leads to the complication of the HP rotor components equilibrium running relationship of an ACE. Meanwhile, it also diversifies the related components matching mechanisms. According to Eq. (24), the first bypass split ratio is the important bond between the HPC and the CDFS.

$$\frac{\mathrm{q}(\lambda_{23})\mathrm{A}_{23}}{\pi_{HPC}} \sqrt{\frac{1}{\eta_{HPT}\left(1-\frac{1}{e_{HPT}}\right)}} \cdot \sqrt{\frac{e_{HPC}-1}{\eta_{HPC}}} = \mathrm{C}_H \tag{40}$$

Although an ACE can operate at four different modes, these modes are relevant to each other. During the mode switch progress, Mode M1 can switch into Mode M13 by turning on the third bypass. Turning on the second bypass can make an ACE switch from Mode M13 to Mode M3. In the same way, if the second bypass is turned on when an ACE operates at Mode M1, its operating mode evolves into Mode 2. Afterwards, Mode M2 can change into Mode M3 by turning on the third bypass. The mode switch relationship between various modes is shown in directly Fig. 4(A).

Analyzing the LP rotor equilibrium running equations at various modes (Eqs. (27), (31), (35) and (38)), It is discovered that the other three LP rotor equilibrium running equations at Mode 1, Mode 13 and Mode 2 are the simplification of the equation at Mode M3. In detail, the LP rotor equilibrium running equation at Mode M3 (Eq. (38)) degenerates into the equation at Mode M2 (Eq. (35)) if the third bypass split ratio is 0. Then, the LP rotor equilibrium running equation at Mode M2 degenerates into the equation at Mode M1 (Eq. (27)) if the second bypass is 0. While, if the second bypass split ratio is 0, the equation at Mode M3 degenerates into the equation at Mode M13 (Eq. (31)). Then, if the third bypass split ratio is 0, the LP rotor equilibrium running equation at Mode M2 degenerates into the equation at Mode M1.

In sum, the differences of these LP rotor equilibrium running equations are embodied in the variations of the three different bypass split ratios. Namely, the Mode M1, the Mode M13 and the Mode 2 can be treated as the special status of the Mode M3. The characteristics of the variations of the LP rotor equilibrium running equations can give expression to the mode switch characteristics of an ACE. The relationships are shown in Fig. 4(B).

3. The ACE performance modeling based on equilibrium running principles

3.1. Introduction to the ACE performance model

As the ACE is a new concept of aero-engine application, in this stage, the ACE components maps utilized in the simulation are not from the rig test. They are from the public reference of USA. As the HPC, CDFS and Flade have related variable geometries, their performance is described by multi-angle maps. For example, the four-angle maps of CDFS are shown in the figure. The angle of VSV_{CDFS} is varied from minimum −45 to maximum 0. This may more or less affect the prediction result. However, during the stage of concept design and preliminary design where real components performance maps are not available, it is a proper way to initiate the ACE performance research which can guide the design and experiments of the components. Then, the components maps through later rig test or CFD with high fidelity can further improve the precision of ACE performance model. These are iterative process.

The ACE performance model calculation flow chart is shown in Fig. 5. This model mainly has two modules: design point calculation module and off-design calculation module. Under the condition of given performance indexes, cycle parameters and other input data, the design point calculation module can confirm aero-engine key geometry parameters, gas thermodynamic parameters of related sections, and other detailed parameters. In others words, design point calculation is to design an ACE via aero-engine size confirmation. Based on the design point calculation, the off design calculation module can calculate the performance parameters and detailed parameters at other operating conditions and operating modes. Steady state calculation and transient state calculation is available in this performance model.

On account of the extremely complexity of an ACE compared with a typical turbofan,its performance model specialties list below:

(1) An ACE has 4 different operating modes;
(2) It adds two compression components: the CDFS and the Flade;
(3) Its matching principle is much more diversiform, as the LP equilibrium running equations vary from different operating modes;
(4) It should consider more static pressure balance relationships;

More variable geometries including the Flade variable stator vane, the CDFS variable stator vane, the HPC variable stator vane, the HPT variable area nozzle, the LPT variable area nozzle, Pro-VABI, Rear-VABI and the engine nozzle area are taken into account which lay the foundation of the wide cycle variation of an ACE.

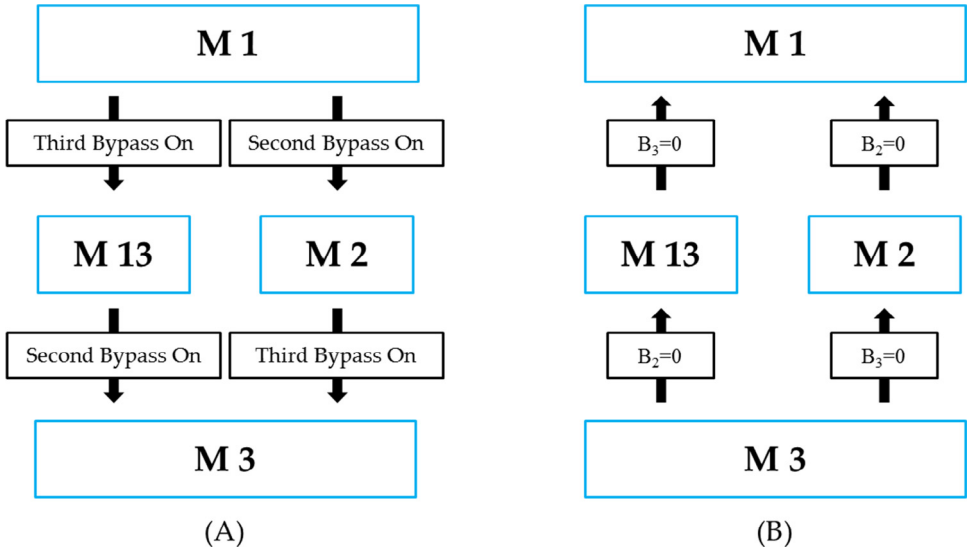

Fig. 4. Variable modes evolution graph. (A) shows the mode switch relationship between various modes. (B) shows the characteristics of the variations of the LP rotor equilibrium running equations.

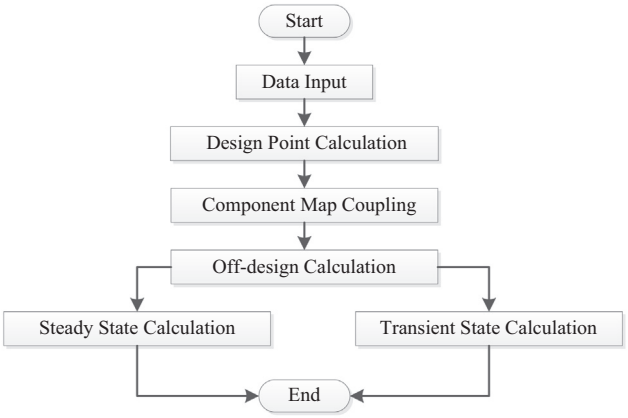

Fig. 5. The ACE performance model calculation flow chart.

Table 2
Important design parameters [12].

Parameter	Value	unit
Height	0	km
Mach number	0	
Working mode	M3	
Specific thrust	96.6	kgf·s/kg
SFC	0.6	kg/(kgf·h)
Total pressure ratio	40	
First bypass split ratio	0.15	
Second bypass split ratio	0.4	
Third bypass split ratio	0.6	
Total bypass split ratio	1.576	

To process the engine design point calculation, the specific parameters should be input beforehand. Some important design parameters at design point are shown in Table 2.

3.2. The equilibrium running equations of the ACE off-design performance calculation

The off-design performance modeling is different with the design point calculation. In terms of the physical essence, the off-design performance calculation is the equilibrium running principles between these components and the specific thermodynamic calculations. In terms of the mathematical calculation, it is nonlinear functions solution which can be regarded as an optimization problem. These functions are on the basis of equilibrium running principles: flow continuity, power balance, pressure balance and rotational speed balance. To mathematical calculation, equilibrium running equations evolve into residual functions. It should be pointed out that the number of residual functions varies from various aero-engines. Generally speaking, a shaft corresponds to two residual functions: a flow continuity function and a power balance function; a mixer corresponds to one pressure balance residual function; a nozzle corresponds to one nozzle throat area balance residual function. So, a conventional double shaft mixed turbofan has 6 functions, a typical double bypass VCE has 7 functions at most (if a VCE operates at single bypass operating mode, it becomes 6 functions). Particularly, the residual functions of an ACE are much more complicated: it has 6 functions at Mode M1, 7 functions at Mode M13 or Mode M2, 8 functions at Mode M3. The details are shown as below.

1. Residual functions of an ACE at Mode M1
   a. Flow continuity residual function of HPT:

$$W_{gc4} - W'_{gc4} = z_1 \tag{41}$$

where W_{gc4} is the HPT inlet corrected gas flow from calculation (kg/s), W'_{gc4} is the HPT inlet corrected gas flow from HPT map (kg/s), z_1 is the first residual value.

   b. Power balance residual function of HP rotor:

$$P_{HPT}\eta_{mH} - P_{HPC} - P_{CDFS} = z_2 \tag{42}$$

where P_{HPT} is the HPT power (W), P_{HPC} is the HPC power (W), P_{CDFS} is the HPC power (W), z_2 is the second residual value.

   c. Flow continuity residual function of LPT:

$$W_{gc5} - W'_{gc5} = z_3 \tag{43}$$

where W_{gc5} is the LPT inlet corrected gas flow from calculation (kg/s), W'_{gc5} is the LPT inlet corrected gas flow from LPT map (kg/s), z_3 is the third residual value.

d. Power balance residual function of LP rotor:

$$P_{LPT}\eta_{mL} - P_{Fan} = z_4 \tag{44}$$

where P_{LPT} is the LPT power (W), η_{mL} is the LP Rotor mechanical efficiency, P_{Fan} is the fan power (W), z_4 is the fourth residual value.

Although the third bypass is just open a little which guarantees the flow continuity at Mode M1, it affects little to the power balance.

e. Static pressure balance residual function of Rear-VABI:

$$p_{s52} - p_{s55} = z_5 \tag{45}$$

where p_{s52} is the mixer bypass inlet static pressure (Pa), p_{s55} is the LPT outlet static pressure (Pa), z_5 is the fifth residual value.

f. Flow continuity residual function of nozzle throat area:

$$A_8 - A'_8 = z_6 \tag{46}$$

where A_8 is the nozzle throat section area from calculation (m^2), A'_8 is the nozzle throat section area from model input (m^2), z_6 is the sixth residual value.

2. Residual functions of an ACE at Mode M13

When an ACE operates at Mode M13, the third bypass is open and the Flade operates. The power balance residual function of LP rotor at Mode 13 (Eq. (47)) is different from the function at Mode M1 (Eq. (44)). In addition, it adds one more residual function (Eq. (48)) which is the flow continuity residual function of third bypass nozzle throat area. The other functions are consistent with the related functions at Mode M1.

$$P_{LPT}\eta_{mL} - P_{Fan} - P_{Flade} = z_4 \tag{47}$$

where P_{LPT} is the Flade power (W).

$$A_{18} - A'_{18} = z_7 \tag{48}$$

where A_{18} is the third bypass nozzle throat section area from calculation (m^2), A'_{18} is the third bypass nozzle throat section area from model input (m^2), z_7 is the seventh residual value.

3. Residual functions of an ACE at Mode M2

When an ACE operates at Mode M2, the second bypass is open. Compared with the residual functions of an ACE at Mode M1, the static pressure residual function of Pro-VABI (Eq. (49)) is considered. The other functions are also consistent with the related functions at Mode M1.

$$p_{s22} - p_{s24} = z_8 \tag{49}$$

where p_{s22} is the second bypass inlet static pressure (Pa), p_{s24} is the first bypass inlet static pressure (Pa), z_8 is the eighth residual value.

4. Residual functions of an ACE at Mode M3

When both the second bypass and third bypass are open at Mode 3, the peculiarities of the residual functions at Mode M13 and Mode 2 are contained in the residual functions at Mode M3. Specifically, the LP rotor power balance residual function is replaced by Eq. (47) compared with the related function at Mode M1 (44). What is more, the residual functions of an ACE at Mode M3 gains Eqs. (48) and (49). The other functions are consistent with the related functions of Mode M1.

The residual values of these above residual functions can form the residual value vector (Eq. (50)). In order to calculate the residual functions set, the corresponding control schedule and the same number of matching guess values is essential. The matching guess values can form the matching guess vector (Eq. (51)). In that way, the nonlinear functions which describe the equilibrium running principles can be expressed by Eq. (52). In a word, the off-design point solution is to solve Eq. (52) in essence.

$$\boldsymbol{Z} = (z_1, z_2, z_3, z_4, z_5, z_6, z_7, z_8)^T \tag{50}$$

where $\boldsymbol{Z}$ is the residual value vector.

$$\boldsymbol{X} = (x_1, x_2, x_3, x_4, x_5, x_6, x_7, x_8)^T \tag{51}$$

where $\boldsymbol{X}$ is the matching guess value vector, x_i is the matching guess value.

$$\boldsymbol{Z}(z_1, z_2, \ldots, z_8)^T = f(\boldsymbol{X}(x_1, x_2, \ldots, x_8)^T) = 0 \tag{52}$$

In order to deal with Eq. (52), the multi-dimensional Newton–Raphson iteration technique is useful. The off-design point calculation flowchart is shown in Fig. 6.

4. Equilibrium running application analysis on various modes of an ACE via the ACE performance model

According to Section 2, the equilibrium running equations at various working modes of an ACE are quite complex due to the three bypass split ratios. So, this section mainly discusses the influences of the three different bypass split ratios to the equilibrium running principles. These principles are useful to the numerical simulation analysis.

The three bypass split ratios have great influence on the cycle variation of an ACE. So, the equilibrium running application analysis is the effects of the referred bypass split ratios variation to the working lines of these related components. The throttling calculation is processed. The working conditions and control schedule of the off-design calculation are shown in Table 3.

The application analysis scheme is shown as below:

Step one: to adjust the three bypass split ratios;
Step two: to calculate the throttling working lines of various components;
Step three: to discuss the three bypass split ratios effects on the equilibrium running equations.

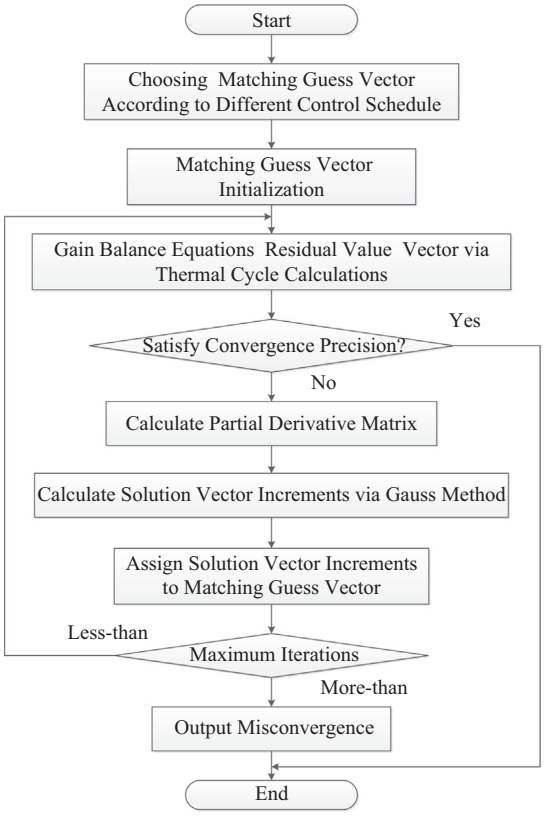

Fig. 6. The off-design point calculation flowchart [12].

Table 3
Working conditions and control schedule.

Parameter	Value	unit
Height	0	km
Mach number	0	
Control variable	LP relative speed	
Throttling original value	1.0	
Throttling stop value	0.7	
Afterburner working condition	No	

The three bypass split ratios analysis should be carried out separately due to the complex the equilibrium running relationships. As the other three LP rotor equilibrium running equations at Mode 1, Mode 13 and Mode 2 are the simplification of the equation at Mode M3, these bypass split ratios analysis can be carried out respectively at specific operating modes.

It is proper to carry out the first bypass split ratio influence analysis at Mode M1 when only the first bypass is open. Similarly, it is suitable to carry out the second bypass split ratio influence analysis at Mode M2 when the second bypass is open but the third bypass is closed. Then, it is suitable to carry out the third bypass split ratio influence analysis at Mode M13 when the third bypass is open but the second bypass is closed. The referred bypass split ratios variations details are shown in Table 4.

It is noteworthy that the three bypass split ratios cannot be adjusted directly. But, they are changed via the variable geometries. The variable geometries are VSV_{Flade}, VSV_{CDFS}, VSV_{HPC}, VAN_{HPT}, VAN_{LPT}, A_8, A_{22} (Pro-VABI) and A_{52} (Rear-VABI). The variable geometries of an ACE are shown in Fig. 7.

The influence analysis of the variable geometries has been carried out deeply in our previous study. The details are discussed systematically in this Ref. [12]. These variable geometries can affect the related bypass split ratios, but they cause other influences. Some can change the related bypass split ratios directly via the flow spilt relationship. Meanwhile, others can change the related bypass split ratios indirectly via the matching mechanism. So, it needs to choose the variable geometries properly.

4.1. The first bypass split ratio effects on equilibrium running principle analysis

The VSV_{HPC} and A_{52} can change the first bypass split ratio directly via the first bypass flow spilt relationship. It is shown in Fig. 8. The variable geometry schedule is shown in Table 5.

Table 4
Bypass split ratio analysis working mode scheme.

Bypass ratio	Working mode
First bypass split ratio	M1
Second bypass split ratio	M2
Third bypass split ratio	M13

Turning up the mixer bypass inlet area (A_{52}) when others remain unchanged at Mode M1 can increase the first bypass gas flow and flow capacity directly. It leads to the increase of the first bypass split ratio. Meanwhile, the CDFS outlet back pressure decreases. Then, the CDFS pressure ratio decreases. They are the direct influences of turning up the mixer bypass inlet area.

With the help of the ACE performance model, the working lines ("Original" and "Adjusted1") of related components are calculated and shown in Figs. 11 and 12. Besides, the first bypass split ratio variation versus the LP relative speed is shown in Fig. 13.

According to the factors influence analysis of Eqs. (21) and (27), the CDFS pressure ratio has negative relationship with the first bypass split ratio. Namely, the increase of the first bypass split ratio leads to the decrease of the CDFS pressure ratio for the equilibrium running relationship. Hence the CDFS working line moves away from the surge line. The relationship is shown in Fig. 9(a). The CDFS working line is shown in Fig. 11(b).

Similarly, the HPC pressure ratio has negative relationship with the first bypass split ratio according to Eqs. (21) and (27). However, it has positive relationship with the first bypass split ratio in Eq. (23). The relationship is shown in Fig. 9(b). So, the HPC working line moves not obviously versus the surge line according. The HPC working line is shown in Fig. 11(c). It moves a little away from the surge line.

According to Eq. (27), the fan pressure ratio has negative relationship with the first bypass split ratio. More specific, the increase of the first bypass split ratio leads to the decrease of the fan pressure ratio for the equilibrium running relationship. Then, the fan

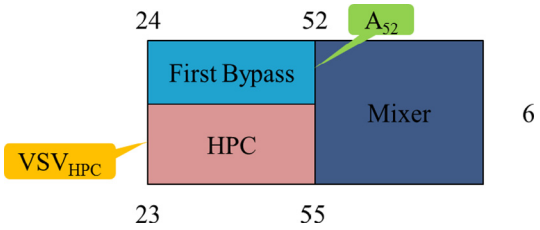

Fig. 8. The first bypass flow spilt relationship diagram.

Table 5
Variable geometry schedule at Mode M1.

Variable Geometry	Original	Adjusted1	Adjusted2
VSV_{Flade} (−85 to 0)	−85	−85	−85
VSV_{CDFS}(−45 to 0)	0	0	0
VSV_{HPC}(−20 to 0)	0	0	−20
A_{22}(0–1.0)[1]	1.0	1.0	1.0
A_{52}(0–1.0)[1]	0.15	0.25	0.15
VAN_{HPT}(0.8–1.2)[1]	1.0	1.0	1.0
VAN_{LPT}(0.8–1.2)[1]	1.1	1.1	1.1
A_8(0.6–1.0)[1]	0.85	0.85	0.85

[1] The value is the ratio of setting area versus design area.

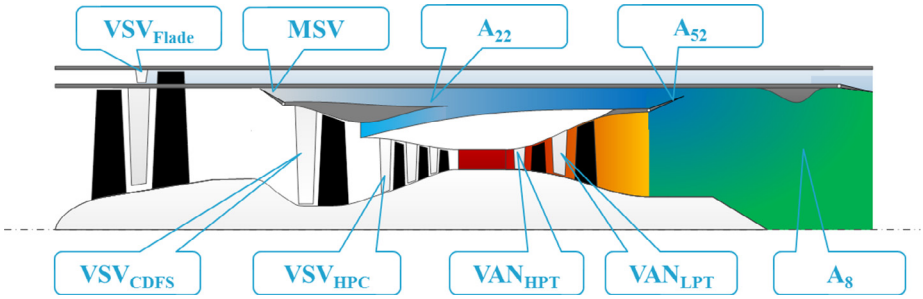

Fig. 7. Variable geometries of an ACE.

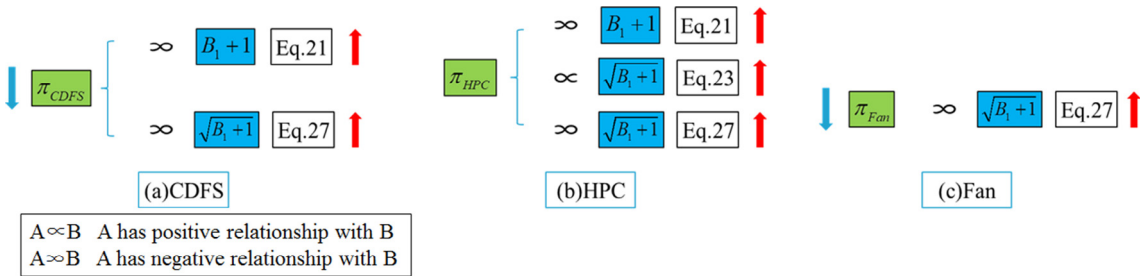

Fig. 9. The related pressure ratio variation relationship when the mixer bypass inlet area is adjusted.

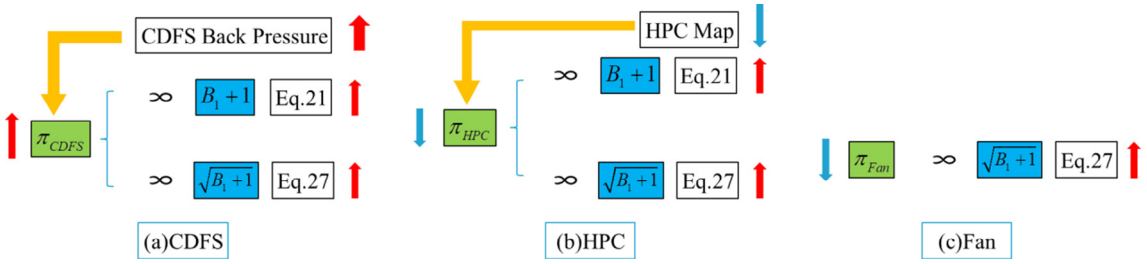

Fig. 10. The related pressure ratio variation relationship when the HPC variable stator vane is adjusted.

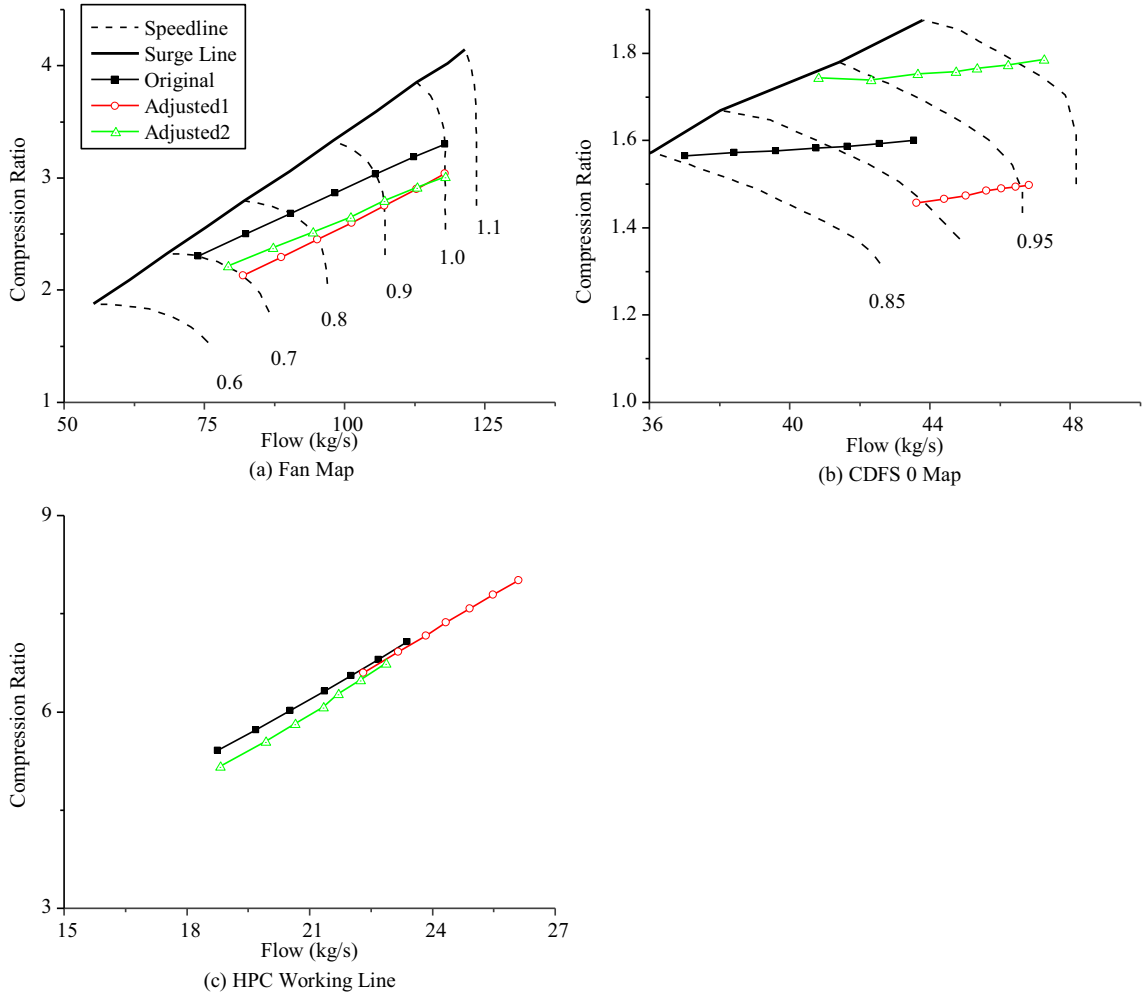

Fig. 11. Working lines of compression components at Mode M1. (a) is the fan working line; (b) is the CDFS working lines at angle 0 map; (c) is the HPC working line. As the HPC variable stator vane is adjusted, the HPC map is a multi-angle map. Thespeed lines and surge lines are not visible in the HPC map.

working line moves away from the surge line. The relationship is shown in Fig. 9(c). The fan working line is shown in Fig. 11(a).

Turning down the HPC variable stator vane when others remain unchanged at Mode M1 can decrease the HPC inlet gas flow and flow capacity directly. The influence of the HPC variable stator vane is more complex. Initially, the HPC component characteristics are changed. The angle −20 HPC map is different from the angle 0 HPC map. Then, it leads to the increase of the first bypass split ratio immediately. Meanwhile, it increases the CDFS outlet back pressure. Although, both the two variable geometries can change the first bypass split ratio. They have other different influences on the matching mechanism of an ACE. Compared with the influences of turning on the mixer bypass inlet area, the CDFS pressure ratio should increase. The working lines (the "Original" and "Adjusted2") of related components are also shown in Fig. 11 and Fig. 12. Besides, the first bypass split ratio variation versus the LP relative speed is shown in Fig. 13.

According to the equilibrium running relationship, the CDFS pressure ratio should decrease when the first bypass split ratio increase. These components matching influences can only weaken the direct influences of the variable geometries adjustments. The variation trends of these direct influences cannot be overturned by the components matching influences. Specifically, the CDFS working line moves close to the surge line, although the first bypass split ratio increases. The CDFS relationship when the HPC variable stator vane is adjusted is shown in Fig. 10(a). The CDFS working line is shown in Fig. 11(b). As the HPC variable stator vane has changed, Eq. (23) cannot be used to discuss the influence. The HPC working line moves away from the surge line more obviously as the HPC map moves down. The increase of the first bypass split ratio lends to the HPC working line moving more away from the surge line. So, the "Adjusted2" line moves more away than the "Adjusted1" line. The HPC relationship when the HPC variable stator vane is adjusted is shown in Fig. 10(b). The HPC working line is shown in Fig. 11(c). The two variable geometries adjustments have the same influences on the fan pressure ratio. So, the two fan working lines both move more away from the surge line.

4.2. The second bypass split ratio effects on equilibrium running principle analysis

The VSV_{CDFS} and A_{22} can change the first bypass split ratio directly via the second bypass flow spilt relationship. It is shown in Fig. 14. The variable geometry schedule is shown in Table 6.

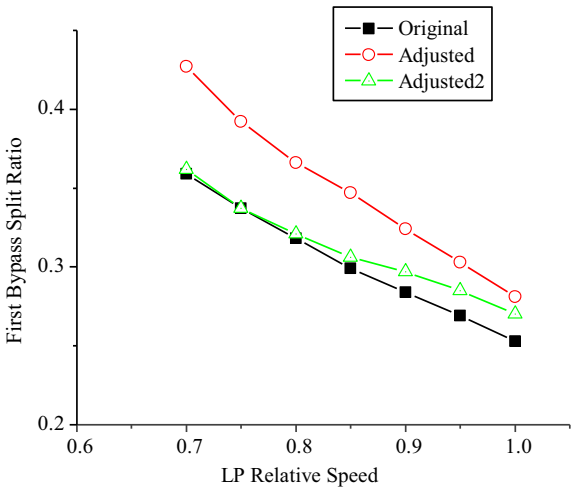

Fig. 13. Variation of first bypass split ratio versus the LP relative speed.

Turning down the CDFS variable stator vane when others remain unchanged at Mode 2 can reduce the CDFS inlet gas flow and the flow capacity directly. The CDFS component characteristics are changed. The second bypass split ratio increases. As the CDFS inlet flow capacity decreases, the fan outlet back pressure increases.

The working lines (the "Original" and "Adjusted1") of related components are calculated and shown in Figs. 17 and 18. Meanwhile, the first and second bypass split ratio variation versus the LP relative speed is shown in Fig. 19.

According to Eq. (35), the first bypass split ratio has negative relationship with the second bypass split ratio. When the second bypass split ratio increases, the first bypass split ratio decreases. It is shown in Fig. 19. The relationship of the first bypass split ratio is shown in Fig. 15(a).

As the CDFS map changes, the CDFS working line moves away from the surge line accordingly. According to Eq. (35), the CDFS pressure ratio has negative relationship with the second bypass split ratio. It causes that the CDFS working line moves more away from the surge line. Due to the equilibrium running relationship, the CDFS pressure ratio should decrease when the second bypass split ratio increase. As the CDFS variable stator vane has changed, Eq. (21) cannot be used to discuss the influence of the first bypass

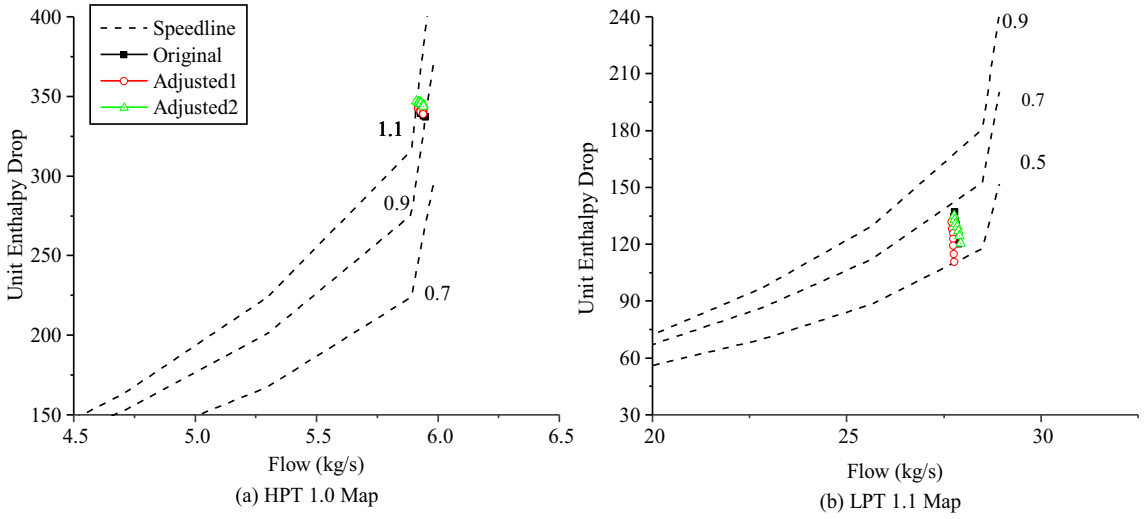

Fig. 12. Working lines of turbine components at Mode M1.

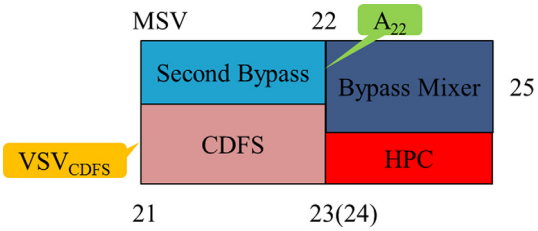

Fig. 14. The second bypass flow spilt relationship diagram.

split ratio. The CDFS pressure ratio influences are shown in Fig. 15 (b). The CDFS working line is shown in Fig. 17(b).

Similarly, the HPC pressure ratio has negative relationship with the second bypass split ratio, according to Eq. (35). The HPC pressure ratio decreases. As the first bypass split ratio decreases, the HPC pressure ratio decreases further. In general, the HPC working line moves away from the surge line. The HPC pressure ratio influences are shown in Fig. 15(c). The HPC working line is shown in Fig. 17(c).

The increase of the fan outlet back pressure leads to the direct increase of the fan pressure ratio. Although the fan pressure ratio has negative relationship with the second bypass split ratio, it can only weaken the increase trend of the fan pressure ratio. So, the fan working line still moves close to the surge line. The fan pressure ratio influences are shown in Fig. 15(d). The fan working line is shown in Fig. 17(a).

Turning down the second bypass outlet area when others remain unchanged at Mode 2 can reduce the second bypass gas flow and the flow capacity directly. Firstly, the second bypass split ratio decreases. For the decline of the second bypass flow capacity, the fan back pressure rises. The fan pressure ratio increases. The lines are marked by "Original" and "Adjusted2" in Figs. 17–19.

When the second bypass split ratio decreases, the first bypass split ratio increases (Fig. 19). The relationship of the first bypass split ratio is shown in Fig. 16(a). According to Eq. (35), the fan pressure ratio has negative relationship with the second bypass split

Table 6
Variable geometry schedule at Mode M2.

Variable geometry	Original	Adjusted	Adjusted2
VSV_{Flade} (−85 to 0)	−85	−85	−85
VSV_{CDFS}(−45 to 0)	−30	−45	−30
VSV_{HPC}(−20 to 0)	−20	−20	−20
A_{22}(0–1.0)[1]	1.0	1.0	0.9
A_{52}(0–1.0)[1]	1.0	1.0	1.0
VAN_{HPT}(0.8–1.2)[1]	1.0	1.0	1.0
VAN_{LPT}(0.8–1.2)[1]	1.0	1.0	1.0
A_8(0.6–1.0)[1]	1.0	1.0	1.0

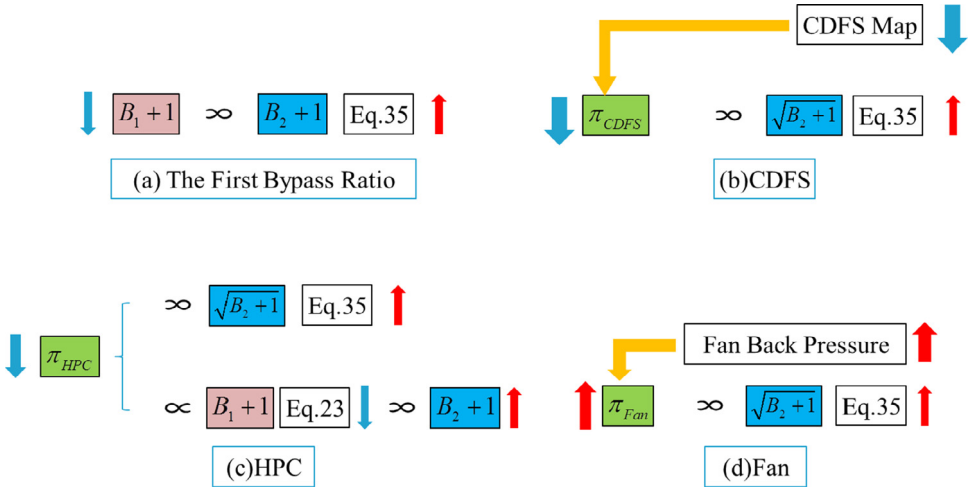

Fig. 15. The related pressure ratio variation relationship when the CDFS variable stator vane is adjusted.

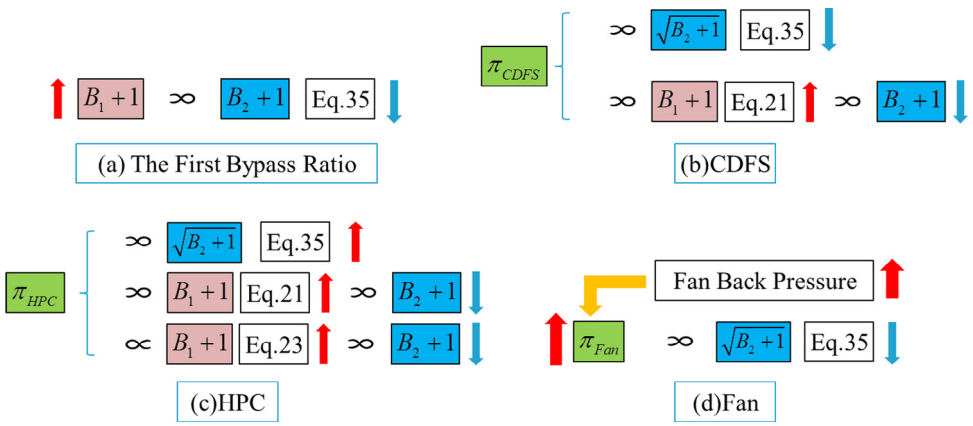

Fig. 16. The related pressure ratio variation relationship when the second bypass outlet area is adjusted.

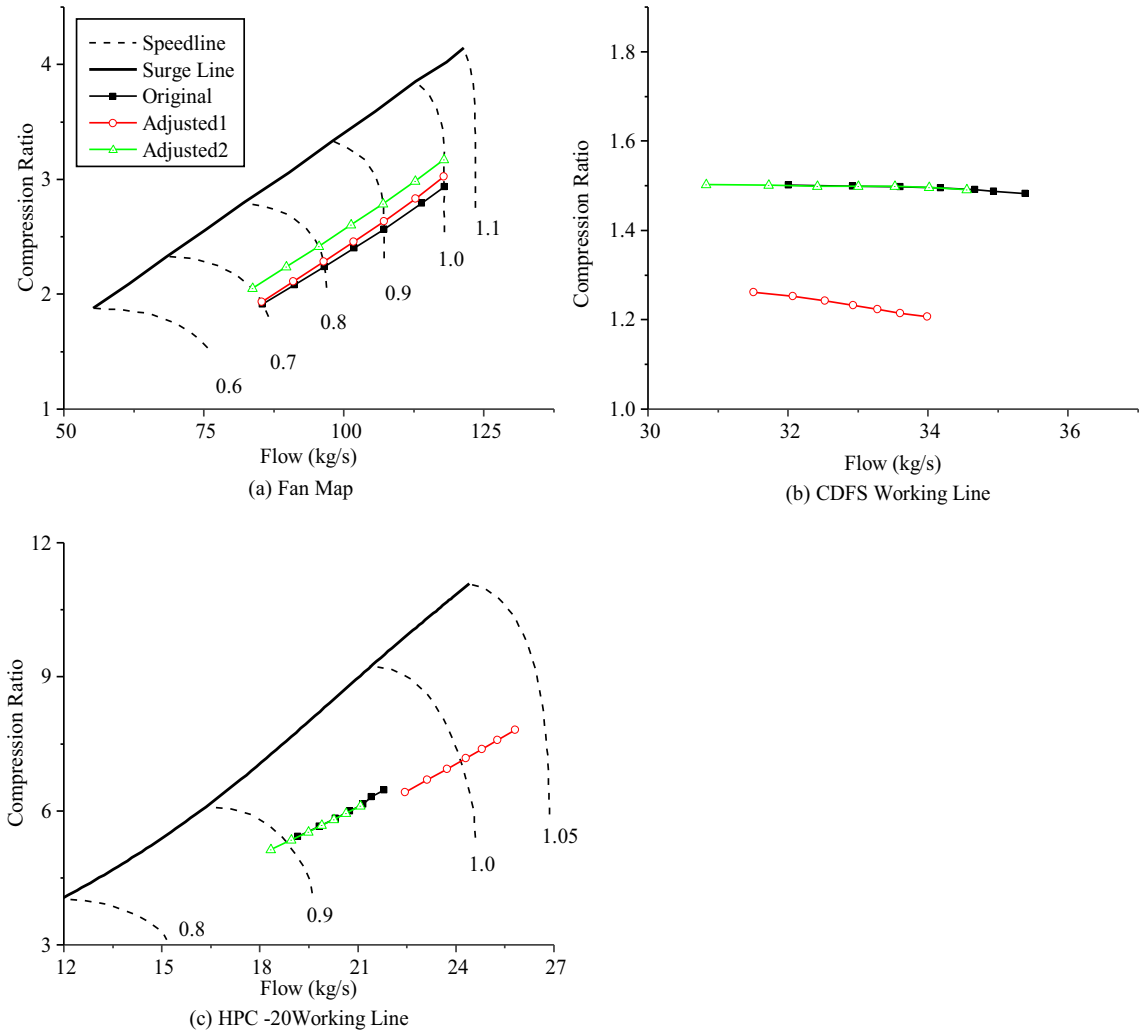

Fig. 17. Working lines of compression components at Mode M2. (a) is the fan working line; (b) is the CDFS working lines; (c) is the HPC working line at angle −20 map. As the CDFS variable stator vane is adjusted, the CDFS map is a multi-angle map. The speed lines and surge lines are not visible in the CDFS map.

ratio. As the second bypass split ratio decreases, the fan pressure ratio increases more. The fan pressure ratio variation relationship is shown in Fig. 16(d). In sum, the fan working line moves more close to the surge line compared with the "Adjusted1" working line in Fig. 17(a). As for the CDFS pressure ratio, it should increase for the negative relationship with the second bypass split ratio

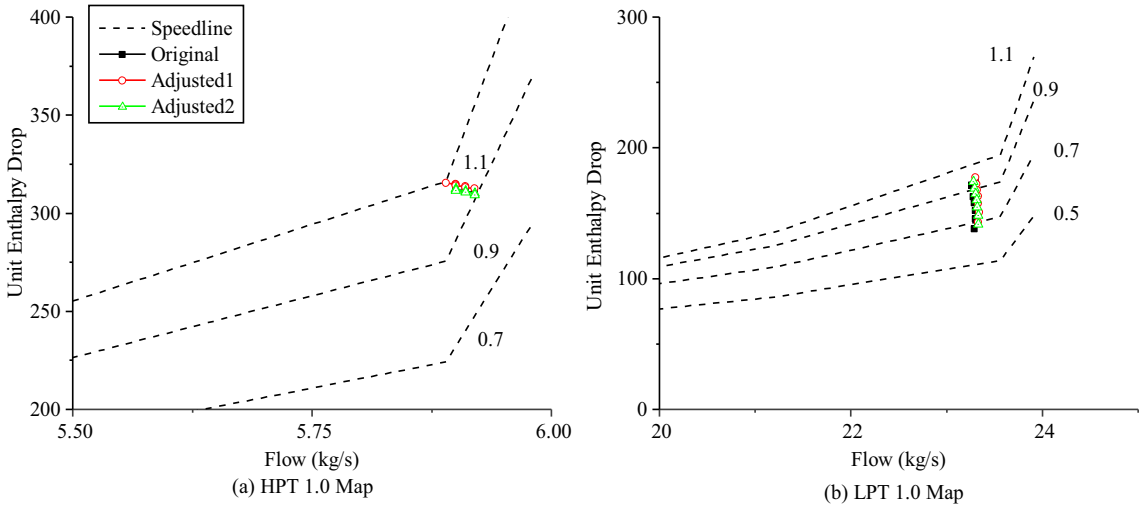

Fig. 18. Working lines of turbine components at Mode M2.

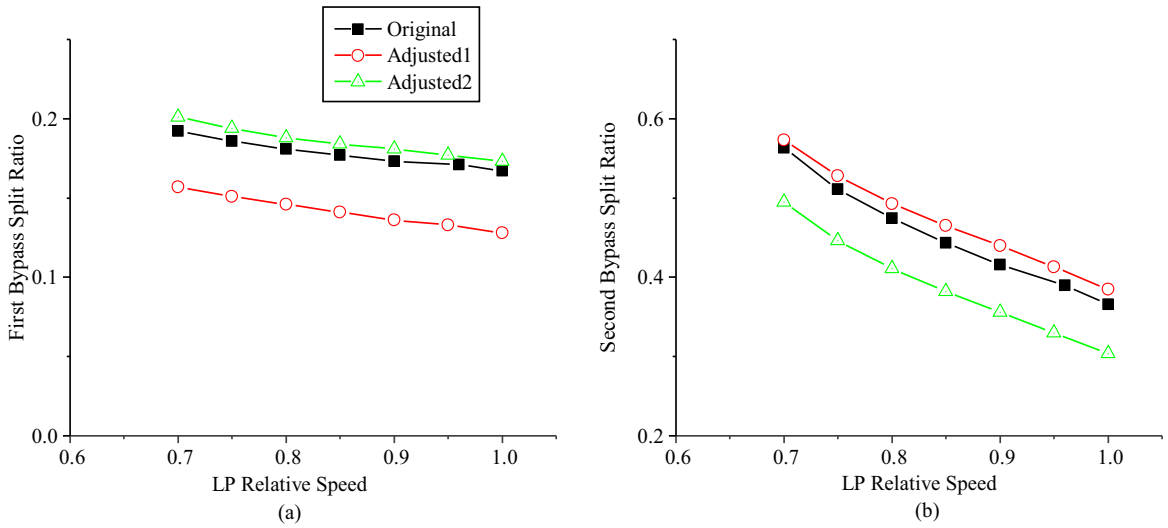

Fig. 19. Variation of the first and second bypass split ratio versus LP relative speed. (a) is the first bypass split ratio variation; (b) is the second bypass split ratio variation.

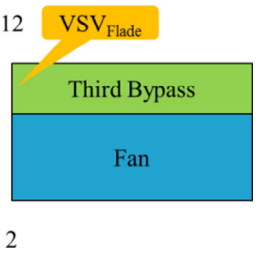

Fig. 20. The third bypass flow spilt relationship diagram.

Table 7
Variable geometry schedule at Mode M13.

Variable geometry	Original	Adjusted
VSV_{Flade} (−85 to 0)	0	−35
VSV_{CDFS}(−45 to 0)	0	0
VSV_{HPC}(−20 to 0)	0	0
A_{22}(0–1.0)[1]	1.0	1.0
A_{52}(0–1.0)[1]	0.2	0.2
VAN_{HPT}(0.8–1.2)[1]	1.0	1.0
VAN_{LPT}(0.8–1.2)[1]	1.1	1.1
A_8(0.6–1.0)[1]	0.85	0.85

according to Eq. (35). On the contrary, it should decrease for the negative relationship with the first bypass split ratio according to Eq. (21). These influences are conflictive which results in little movement versus the surge line of the CDFS working line (shown in Fig. 17(b)). The CDFS pressure ratio variation relationship is shown in Fig. 16(b). According to Eq. (35), the HPC pressure ratio has negative relationship with the second bypass split ratio. Besides, the HPC pressure ratio has negative relationship with the first bypass split ratio according to Eq. (21). However, it has positive relationship with the first bypass split ratio according to Eq. (23). Namely, the HPC working line remains little movement versus the surge line. This is shown in Fig. 17(c). The HPC pressure ratio variation relationship is shown in Fig. 16(c).

4.3. The third bypass split ratio effects on equilibrium running principle analysis

As the fan stator vane is fixed, only the VSV_{Flade} can change the third bypass split ratio directly via the third bypass flow spilt relationship. The flow spilt relationship is shown in Fig. 20. The variable geometry schedule is shown in Table 7.

Turning down the Flade variable stator vane when others remain unchanged at Mode M13 can decrease the Flade inlet air flow and flow capacity directly. Furthermore, the Flade component characteristics are changed. It is noteworthy that the air flow of the third bypass doesn't mix with the main nozzle. The Flade only changes the LP power balance. Although the Flade variable stator vane is changed, Eq. (32) is still useful. As the third bypass ratio multiplies by a micro variable in Eq. (31), this equation cannot reflect the relationship between the third bypass split ratio and other factors.

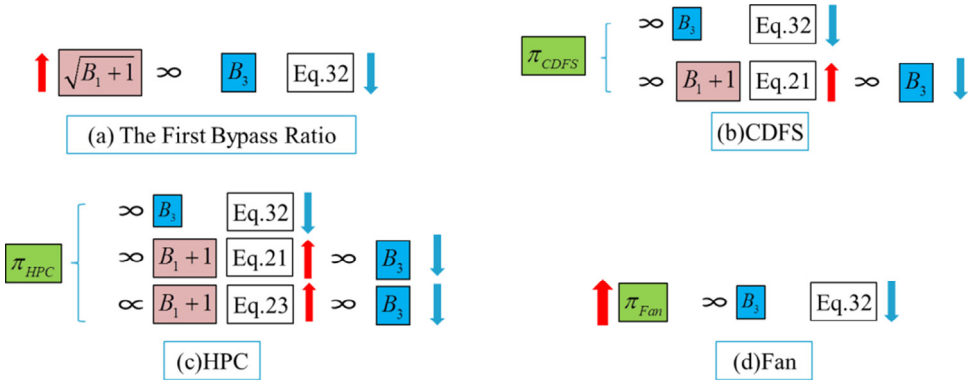

Fig. 21. The related pressure ratio variation relationship when the Flade variable stator vane is adjusted.

According to Eq. (32), the first bypass split ratio has negative relationship with the third bypass split ratio. When the third bypass split ratio decreases, the first bypass split ratio increases. It is shown in Fig. 24. The relationship of the first bypass split ratio is shown in Fig. 21(a). The working lines of HPT and LPT are shown in Fig. 23.

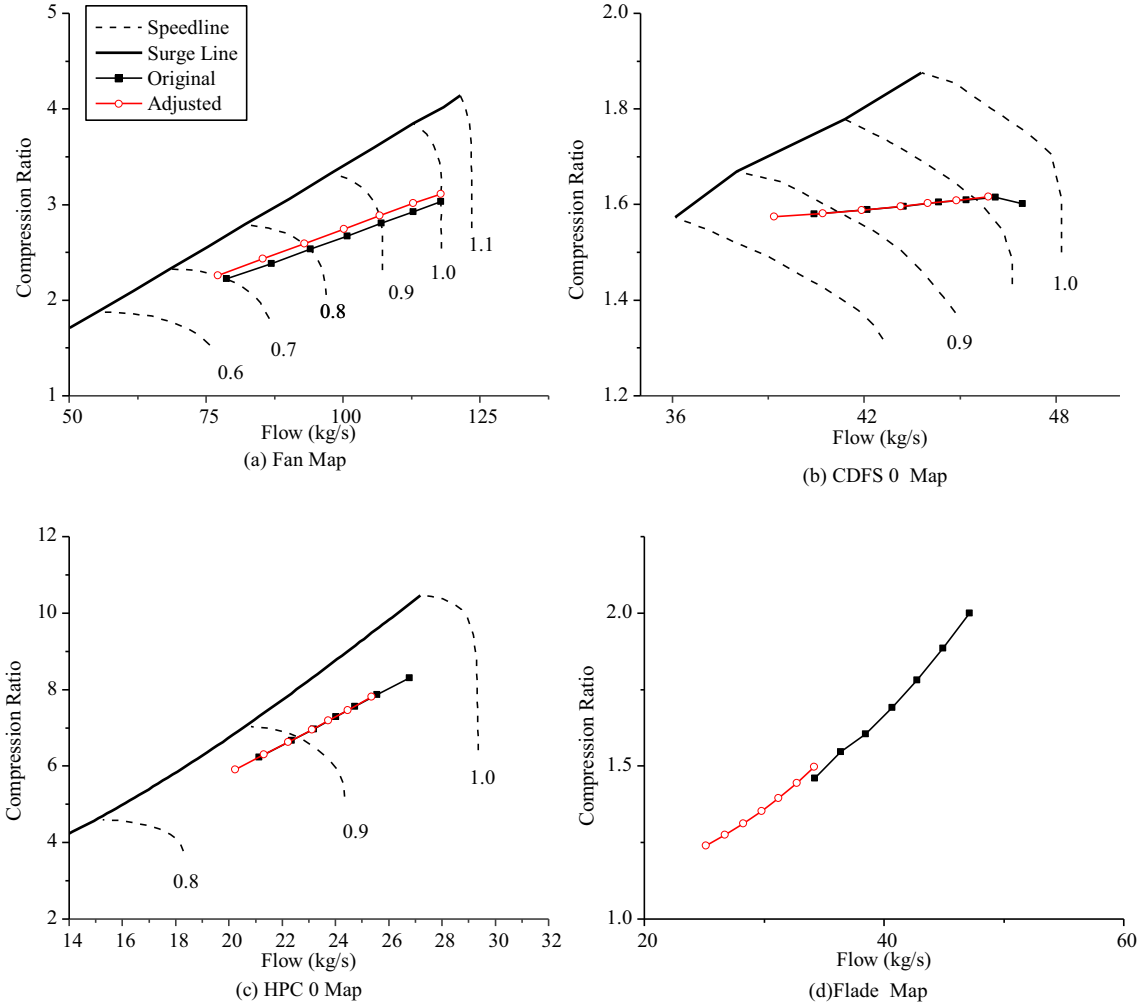

Fig. 22. Working lines of compression components at Mode M13. (a) is the fan working line; (b) is the CDFS working lines at angle 0 map; (c) is (c) is the HPC working line at angle 0 map; (d) is the Flade working lines. As the Flade variable stator vane is adjusted, the Flade map is a multi-angle map. The speed lines and surge lines are not visible in the Flade map.

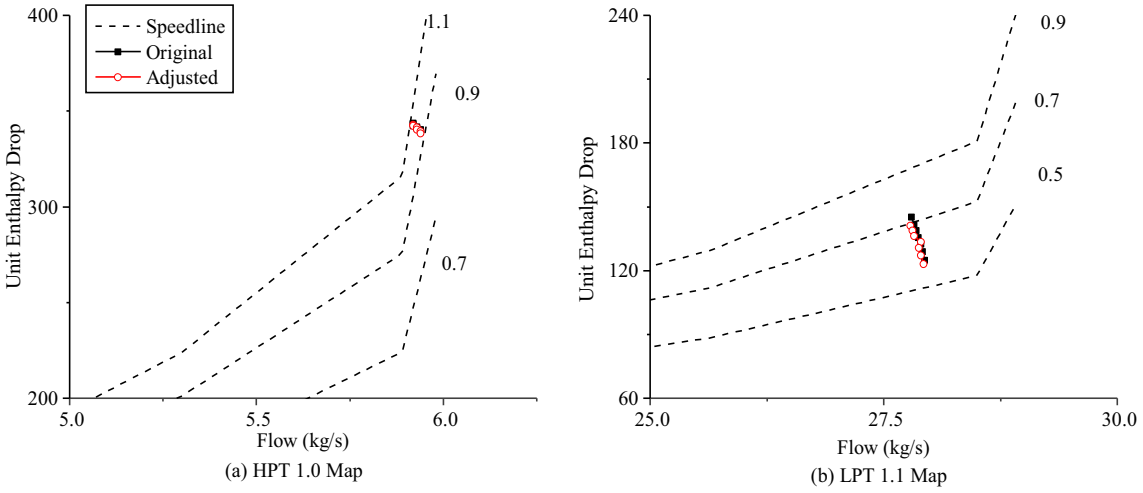

Fig. 23. Working lines of turbine components at Mode M13.

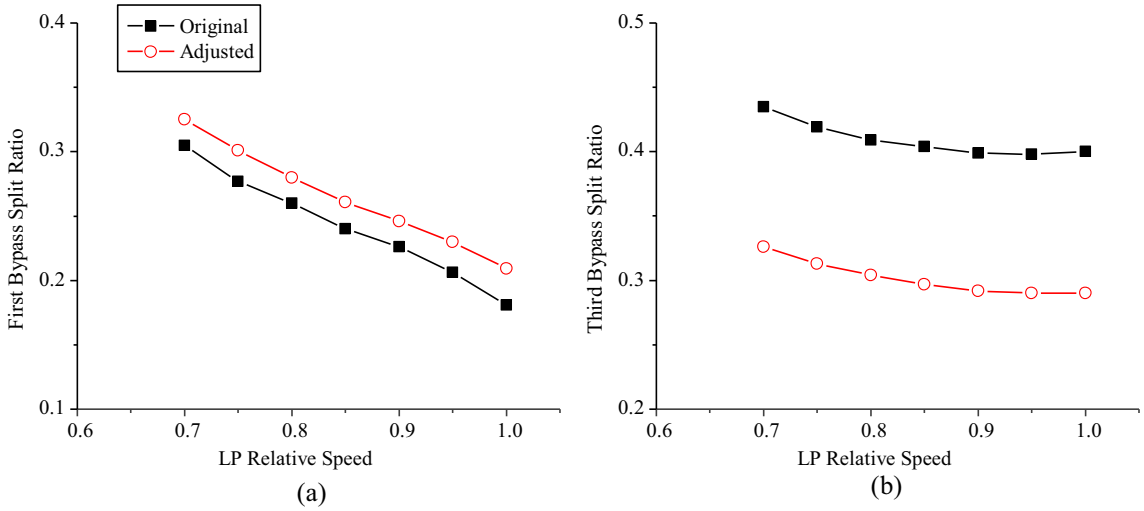

Fig. 24. Variation of the first and third bypass split ratio versus LP relative speed. (a) is first bypass split ratio variation; (b) is third bypass split ratio variation.

The CDFS compression ratio should increase when the third bypass split ratio decreases. But the first bypass split ratio also increases. It should decrease for the negative relationship with the first bypass split ratio according to Eq. (21). So, the CDFS working line remains little movement versus the surge line which is shown in Fig. 22(b). The CDFS pressure ratio variation relationship is shown in Fig. 21(b).

According to Eq. (32), the HPC pressure ratio has negative relationship with the third bypass split ratio. Then, the HPC pressure ratio has negative relationship with the first bypass split ratio according to Eq. (21). However, it has positive relationship with the first bypass split ratio according to Eq. (23). Namely, the HPC working line also remains little movement versus the surge line which is shown in Fig. 22(c). The HPC pressure ratio variation relationship is shown in Fig. 21(c).

The fan pressure ratio has negative relationship with the third bypass split ratio according to Eq. (35). So, the fan working line moves close to the surge line. The related figures are Fig. 21(d) and Fig. 22(a).

5. Conclusions

This paper uncovers the physical essence of components matching relationships and provides mathematical derivation of equilibrium running principles. It lays the theoretical foundation on the variable geometries modulation schedule and performance analysis on an ACE. According to these principles, the advantages of an ACE such as the wide variable cycle characteristics will be discovered more perfectly. The conclusions are drawn as below:

1. Compared with the conventional double shaft mixed turbofan HP rotor equilibrium running equation, the HP rotor equilibrium running equation of an ACE gains additional factors: the CDFS and the first bypass split ratio. The first bypass split ratio leads to the complication of the HP rotor components equilibrium running relationship of an ACE. Meanwhile, it also diversifies the related components matching mechanisms and is the important bond between the HPC and the CDFS.
2. The LP rotor equilibrium running equations at Mode M1, M13 and M2 are the simplifications of the equilibrium running equation at Mode M3. The differences of these LP rotor equilibrium running equations are embodied in the variations of the three different bypass split ratios. The Mode M1, the Mode M13 and the Mode 2 can be treated as the special status of the Mode M3. The characteristics of the variations of the LP rotor equilibrium running equations can give expression to the mode switch characteristics of an ACE.
3. The variations of the first, second and third bypass split ratios lay the foundation of the wide cycle variation of an ACE. The first, second and third bypass split ratios are the core influences on components matching relationships and the equilibrium running principle. The three bypass split ratios can be changed passively via the variable geometries. According to the equilibrium running principles, the first bypass split ratio has negative relationship with the second and third bypass split ratios.
4. Turning up the mixer bypass inlet area or turning down the VSV_{HPC} can increase the first bypass split ratio. Besides, the fan and HPC working line moves away from the surge line. The CDFS working line moves away from the surge line on account of the former adjustment while it moves on the contrary due to the latter. Turning down the VSV_{CDFS} can increase the second bypass split ratio while turning up the second bypass outlet area can decrease it. Due to the two adjustments, the fan working line moves close to the surge line. The former adjustment leads to the movement of the HPC and CDFS working lines away from their surge lines. However, the latter hardly affects the two working lines. Turning down the VSV_{Falde} can decrease the third bypass split ratio. This adjustment can only affect the fan working line while the CDFS and HPC working lines are scarcely impacted.

Acknowledgments

This work was supported by the Natural Science Foundation of China (NSFC) under Grants #51206005 and #51776010.

Appendix A. Supplementary material

Supplementary data associated with this article can be found, in the online version, at https://doi.org/10.1016/j.applthermaleng.2017.12.102.

References

[1] P. Pilidis, Predicted performance characteristics of a variable cycle turbofan, Aeronaut. J. 101 (1997).
[2] J. Kurzke, The mission defines the cycle: turbojet, turbofan and variable cycle engines for high speed propulsion, Vki Lecture (2010).

[3] M.H. Sadraey, Aircraft design: a systems engineering approach, Aircraft Design: A Systems Engineering Approach, Wiley, 2012.
[4] O. Balli, Exergy modeling for evaluating sustainability level of a high by-pass turbofan engine used on commercial aircrafts, Appl. Therm. Eng. 123 (2017).
[5] A.F. Woolf, Conventional prompt global strike and long-range ballistic missiles: background and issues, Congr. Res. Serv. Rep. (2011).
[6] C. Salpingidou, Z. Vlahostergios, D. Misirlis, et al., Thermodynamic analysis of recuperative gas turbines and aero engines, Appl. Therm. Eng. 124 (2017).
[7] J. Johnson, Variable cycle engines – the next step in propulsion evolution, in: 12th Propulsion Conference AIAA, 1976.
[8] W.W. Thomas, E.V. Sprunger, Two-spool variable cycle engine: US, US4043121 [P], 1977.
[9] C.D. Wagenknecht, G.K. Faust, Individual bypass injector valves for a double bypass variable cycle turbofan engine: US, US4175384[P], 1979.
[10] G.D. Roberge, Auxiliary propulsor for a variable cycle gas turbine engine: US, US8127528[P], 2012.
[11] B. Li, M. Chen, Z.L. Zhu, Steady performance investigation at various modes of an adaptive cycle aero-engine, J. Propul. Technol. 34 (8) (2013) 1009–1015 [Chinese].
[12] J. Zheng, M. Chen, H. Tang, Matching mechanism analysis on an adaptive cycle engine, Chin. J. Aeronaut. 30 (2) (2017) 706–718.
[13] Y. Lyu, H. Tang, M. Chen, A study on combined variable geometries regulation of adaptive cycle engine during throttling, Appl. Sci. – Basel 6 (12) (2016) 374.
[14] G. Gonca, B. Şahin, Thermo-ecological performance analyses and optimizations of irreversible gas cycle engines, Appl. Therm. Eng. 105 (2016) 566–576.
[15] Xiangxing Kong, Xi Wang, Daoliang Tan, An extrapolation approach for aeroengine's transient control law design, Chin. J. Aeronaut. 26 (5) (2013) 1106–1113.
[16] M. Chen, Z.L. Zhu, D.M. Zhu, et al., Performance analysis tool for turbine based combined cycle engine concept, J. Astro. 27 (5) (2006) 854–859 [in Chinese].
[17] NATO, Performance prediction and simulation of gas turbine engine operation for aircraft, Marine, Vehicular, and Power Generation, RTO, R-AVT-036, 2007.
[18] M. Chen, H.L. Tang, H. Zhang, Turbine based combined cycle propulsion system integration concept design, J. Aerosp. Eng. Proc. Inst. Mech. Eng. Part G. V227 (7) (2012) 1068–1089.
[19] H.L. Tang, M. Chen, et al., High altitude low Reynolds number effect on the matching performance of a turbofan engine, J. Aerosp. Eng. Proc. Inst. Mech. Eng. Part G: J. Aerosp. Eng. v227 (3) (2013) 455–466.
[20] M. Chen, Z.L. Zhu, Goal programming for stable mode transition in tandem turbo-ramjet engines, Chin. J. Aeronaut. 05 (2009) 486–492.